Biomaterials 256 (2020) 120195

Contents lists available at ScienceDirect

Biomaterials

journal homepage: www.elsevier.com/locate/biomaterials

Engineering anisotropic human stem cell-derived three-dimensional cardiac tissue on-a-chip

Jaimeson Veldhuizen[a], Joshua Cutts[a], David A. Brafman[a], Raymond Q. Migrino[b,c], Mehdi Nikkhah[a,d,*]

[a] School of Biological and Health Systems Engineering, Arizona State University, Tempe, AZ, 85287, USA
[b] Phoenix Veterans Affairs Health Care System, Phoenix, AZ, 85022, USA
[c] University of Arizona College of Medicine, Phoenix, AZ, 85004, USA
[d] Biodesign Virginia G. Piper Center for Personalized Diagnostics, Biodesign Institute, Arizona State University, Tempe, AZ, 85287, USA

ARTICLE INFO

Keywords:
Stem cell
Cardiac
Microenvironment
Myocardium
Microfluidic chips

ABSTRACT

Despite significant efforts in the study of cardiovascular diseases (CVDs), they persist as the leading cause of mortality worldwide. Considerable research into human pluripotent stem cell-derived cardiomyocytes (hPSC-CMs) has highlighted their immense potential in the development of *in vitro* human cardiac tissues for broad mechanistic, therapeutic, and patient-specific disease modeling studies in the pursuit of CVD research. However, the relatively immature state of hPSC-CMs remains an obstacle in enhancing clinical relevance ofengineered cardiac tissue models. In this study, we describe development of a microfluidic platform for 3D modeling of cardiac tissues, derived from both rat cells and hPSC-CMs, to better recapitulate the native myocardium through co-culture with interstitial cells (specifically cardiac fibroblasts), biomimetic collagen hydrogel encapsulation, and induction of highly anisotropic tissue architecture. The presented platform is precisely engineered through incorporation of surface topography in the form of staggered microposts to enable long-term culture and maturation of cardiac cells, resulting in formation of physiologically relevant cardiac tissues with anisotropy that mimics native myocardium. After two weeks of culture, hPSC-derived cardiac tissues exhibited well-defined sarcomeric striations, highly synchronous contractions, and upregulation of several maturation genes, including HCN1, KCNQ1, CAV1.2, CAV3.1, PLN, and RYR2. These findings demonstrate the ability of the proposed engineered platform to mature animal- as well as human stem cell-derived cardiac tissues over an extended period of culture, providing a novel microfluidic chip with the capability for cardiac disease modeling and therapeutic testing.

1. Introduction

Heart disease remains the leading cause of mortality, despite abundant advancements in cardiovascular research [1]. Research involving animal models has contributed significantly to cardiovascular disease-related knowledge gathered to date, however challenges remain in translating preclinical findings to human conditions due to pronounced physiological differences [2]. Additionally, inherent difficulties in studying the heart *in vivo* at cellular and molecular levels hinder the discovery and extensive study of disease-specific mechanisms. In the past few years, synergistic *in vitro* models using human cells/tissues that enable detailed mechanistic studies of cell-cell and cell-environment interactions have served to complement *in vivo* preclinical findings [3–7]. *In vitro* research based on the use of human cardiac cells is now more accessible, due to advances in the development of robust and reproducible methods for directed differentiation of high yield human stem cell-derived cardiomyocytes (CMs), from both human embryonic stem cells (hESCs) and human induced pluripotent stem cells (hiPSCs), referred to collectively as hPSCs [8]. Particularly, methods to purify differentiated cardiac populations for CMs [9], including magnetic-activated cell sorting (MACS) [10], fluorescence-activated cell sorting (FACS) [11], and metabolic selection [12], have enabled consistent yields of highly pure CM populations, that have been extensively used, among many other applications, to engineer *in vitro* human cardiac tissue models for mechanistic, disease-specific, and therapeutic research. However, although CMs comprise most of the volume, cardiac fibroblasts (CFs) constitute a majority of the cell population within the heart [13], resulting in structural misalignment within the majority of

* Corresponding author. School of Biological and Health Systems Engineering, Arizona State University, Tempe, AZ, 85287, USA.
E-mail address: mnikkhah@asu.edu (M. Nikkhah).

https://doi.org/10.1016/j.biomaterials.2020.120195
Received 16 January 2020; Received in revised form 15 May 2020; Accepted 9 June 2020
Available online 26 June 2020
0142-9612/

in vitro studies that rely on mono-culture of hPSC-CMs. Some studies continue to use unpurified hPSC-CM populations to address the need for multi-culture populations [14,15], that include interstitial non-CM cells, such as fibroblasts, smooth muscle cells, and endothelial cells at differing ratios. However, CM purity and cellular composition have proven quite difficult to control during human stem cell differentiation, resulting in extensive variation in cellular composition of heart tissues in models that utilize mono-culture of unpurified hPSC-CMs. Therefore, there is a need for the incorporation of controlled and consistent co- or multi-culture ratios of purified CMs and supporting interstitial cells within *in vitro* platforms to better recapitulate the native architecture and function of human myocardium.

The complex cellular composition within intricate architecture in the native myocardium is necessary for highly synchronous organ-level contraction [16]. During myocardial development, CMs are exposed to physical, electrical, and mechanical stimuli that enhance organization of overall tissue structure, promote cell elongation and increase cell length-to-width ratios, thereby influencing intracellular contractile machinery, including alignment of sarcomeres and localization of gap junctions [17]. Due to these stimuli, the muscle fibers arrange in a parallel array, and the cells organize in an anisotropic manner, with electromechanical connections forming through intercalated discs at the perpendicular edges. To that end, it is crucial to recapitulate the native-like 3D tissue anisotropy within engineered *in vitro* tissue models for physiologically relevant cellular- and molecular-level studies. Previous studies have utilized numerous strategies to align cardiac tissues by simulating relevant stimuli that are experienced by the native myocardium, including environmental cues, such as micropatterned substrates [18] or surface topography [14,19], mechanical tension and electrical stimulation [15,18,20,21].

Another current obstacle for clinical translation of *in vitro* platforms is the relatively immature state of hPSC-CMs, evidenced by round cell morphology, lack of mature contractile machinery, and gene expression profiles resembling fetal CMs [22–28]. To enhance clinical relevance and future translation of stem cell-derived CMs, a multitude of techniques have been investigated to aid in their maturation [24]. These methods range from applied stimulation, i.e. electrical or mechanical [20,29]; culture variation, i.e. long-term culture [28], media supplementation [30], or co-culture with non-CMs [31]; or environmental cues, i.e. extracellular matrix (ECM) [32], mesoscopic architecture [14,19], or micropatterned substrates [33]. The CM populations that result from these methods exhibit more mature structure and function, evidenced through enhanced morphology, function, protein and gene expression, and electrophysiology. Recent *in vitro* studies have utilized some of these maturation techniques to model more adult-like cardiac tissues from hPSC-derived CMs within complex biomimetic platforms [34]. Such platforms include 3D anisotropic patches [19], flexible thin films [18], electrically-stimulated biowires [20], engineered heart tissues (EHT) suspended between micropillar arrays [21], as well as heart-on-a-chip tissues within microfluidics [35–37]. Among these engineered cardiac tissues, incorporation of microfluidic technology retains certain advantages for organ modeling, mainly due to precise control over diffusion of gradients (i.e. drug or chemical) and cell culture environment, low cost and ease of manufacture, and requirement for minimal quantity of tissues and corresponding reagents [35–37]. Due to the minimal cell and low-cost requirements involved in manufacture of each microfluidic device, a multitude of devices can be incorporated simultaneously to facilitate high throughput experimentation. This allows for a single batch of differentiated stem cell-derived CMs to be utilized for the same set of experiments, reducing variability from interdifferentiation population differences [38] that may obscure underlying biological results.

To date, notable progress has been made in engineering *in vitro* cardiac tissue models using microfluidic platforms [35,36,39]. Similar to macroscale approaches, microfluidic cardiac tissues have also been formed both with and without scaffolds. The related advantages and disadvantages of scaffold-based vs. scaffold-free approaches, that have been discussed extensively [40], can also be applied to tissues created at the microscale. Despite significant findings of both approaches using microfluidics, many *in vitro* platforms have incorporated mono-culture of hPSC-CM populations to specifically model 3D myocardial tissue. In addition, the majority of these studies have characterized the functionalities of the engineered micro-tissues through immunofluorescence, drug responsiveness, and force generation, to provide important information about the engineered tissue structure and function. To further enhance these findings, it is critical to additionally perform extensive molecular-level studies, including protein or gene expression analyses, in comparison to age-matched cell populations. Such validation of the resultant tissues generated within micro-engineered models is crucial for their effective translation in future disease-specific and therapeutic studies. Furthermore, as the anisotropic architecture of the myocardium is pertinent for its proper function, some of these microfluidic models utilize ECMcoating and confined features to create aligned cardiac tissues [36]. To better mimic the inherent 3D extracellular matrix and fibers of the native myocardium, there is a need for incorporation of aligned 3D cardiac tissues within microfluidic platforms.

In this study, we demonstrate the development of a novel microfluidic platform precisely designed and further characterized with three distinct cell types, to induce anisotropy of co-cultured 3D hydrogel-encapsulated cardiac tissues, while enabling enhanced nutrient diffusion through the creation of repeated elliptical pores [41]. Specifically, surface topography was incorporated within the central 3D tissue region of the microfluidic platform, in the form of staggered microposts, to mimic the anisotropic structure of the human native myocardium, serving to further enhance physiological relevance of our model. In addition, to better control the composition and reduce variation among cardiac tissues from different differentiation batches, we utilized a metabolic purification protocol to select for high percentages of CMs from hPSC-derived populations. The highly pure CM populations ($85.5 \pm 5.3\%$ $cTnT^+$) were further co-cultured with human CFs at a consistent ratio (4:1 CM:CF), encapsulated in a hydrogel, and housed within the 3D microfluidic device to generate biomimetic myocardial tissue. The microfluidic nature of the platform enabled establishment of exact temporal and spatial gradients for possible future drug-related studies, while maintaining a minimal cell and reagent requirement (i.e. 3 μL of cell:hydrogel suspension per device) for optimal experimental design. Cardiac tissues formed within the designed microfluidic chip were reproducibly generated from three distinct cell types, and presented enhanced mature cellular structure, protein expression, gene expression and tissue function.

2. Materials and methods

2.1. Microfluidic device fabrication

Photolithography and replica molding technique were used to create the microfluidic devices, consistent to our previous work [42–45], composed of staggered elliptical microposts within the main 3D tissue region, bordered by arrays of trapezoidal microposts. Briefly, SU8 2075 was spin-coated to 200 μm on a 4" silicon wafer. The wafer was exposed to ultraviolet light through a transparent mask of the microfluidic channel design (created in AutoCAD). After development of the SU8, the wafer was prepared for polydimethylsiloxane (PDMS, Essex Brownell) replica molding via silanization, using methyltrichlorosilane (MTCS), of the surface to reduce attraction between cast PDMS and SU8 features. PDMS base and crosslinker were mixed at a 10:1 ratio and poured on the master silicon wafer. After 1.5 hr of curing at 80 °C, the PDMS mold was peeled and holes for the inlets and outlets of the tissue and media channels were made with biopsy punches (1 mm for tissue channel and 1.5 mm for media channels). The PDMS channels were then bonded to 18 × 18 mm coverslips with oxygen

plasma (PDC-32G, Harrick Plasma), and baked at 80 °C overnight to secure bonds. The devices were sterilized via two cycles of autoclave, first through liquid cycle and then through gravity cycle. The devices were baked at 80 °C overnight to ensure dehydration before use in cell culture experiments.

2.2. Diffusion analysis through the 3D cardiac tissue region

Simulation of diffusion of 10 kDa FITC-Dextran through the 3D cardiac tissue region was performed with COMSOL Multiphysics. With the assumption that the gel is uniform in the z-direction, simulation of diffusion was only performed in the x-y region [42]. Using the Stokes-Einstein equation $D = (kT)/(6\eta\pi R)$ [46] where D is diffusion coefficient, R is stokes radius (69 Å), T is temperature (310.15K), k is the Boltzmann coefficient ($1.38*10^{-23}$ J/K), and η is the dynamic viscosity of media at 37 °C ($0.78*10^{-3}$ N*s/m^2) [47], the value for the diffusion coefficient of 10 kDa of FITC-Dextran in media at 37 °C was found to be $4.22*10^{-12}$ m^2/s. In order to determine the diffusion coefficient of the tissue region, the diffusion hindrance coefficient was determined as 0.94 with the main hydrogel component as collagen type 1 (2 mg/mL), therefore the diffusion coefficient for media was multiplied by 0.94 [42], to find the diffusion coefficient of the hydrogel to be $3.97*10^{-12}$ m^2/s. The concentration of dextran within the media channels was set to 10 μg/mL, and the tissue channel at t = 0 to be 0 μg/mL.

2.3. Neonatal rat cardiac cell isolation and culture

Neonatal ventricular rat-derived cardiomyocytes (rCMs) and cardiac fibroblasts (rCFs) were obtained from two-day old neonatal rats based on a well-defined protocol approved by Institution of Animal Care at Arizona State University, as demonstrated in our earlier work [33,48–51]. The thorax of the rats was opened and the heart was surgically removed. Upon removing the atria, the hearts were cut into 3–4 medium sized pieces and placed in 0.05% trypsin solution (without EDTA; Gibco) prepared in Hank's balanced salt solution (HBSS; Gibco) for 14–16 hr at 4 °C with continuous gentle agitation. After trypsination, the heart pieces were neutralized in cell culture media and further subjected to collagenase treatment to digest the ECM and isolate the cells, comprised mainly of rCMs and rCFs. The cell suspension was preplated and the cells left to attach for an hour. The suspended cells were collected, as the rCMs, and the attached cells were isolated as the rCFs. The rCMs and rCFs were immediately used for device culture. Both cell types were suspended for a final density of $30x10^6$ cells/mL and mixed to desired ratio (i.e. 1:0, 8:1, or 4:1 CM:CF), then this cell mixture was mixed with bovine thrombin, bovine fibrinogen, and rat tail collagen type 1 (Corning), for a final concentration of fibrin (2 mg/mL) and collagen (1 mg/mL) at a ratio of 85:15. The cell:hydrogel solution was injected into the microfluidic device, flipped and polymerized at 37 °C for 18 min, then media (DMEM 1X, 10% FBS, 1% Pen/strep, 1% L-glutamine) was added to the side channels. Media was changed daily.

2.4. Human stem cell culture

hESCs, that were edited through delivery of a plasmid encoding GFP under the hTNNT2 promoter, were received as a generous gift from Dr. David Brafman's lab (ASU). hiPSCs (cell line: SCVI20) were purchased from Stanford Cardiovascular Institute Biobank. Pluripotency of hPSC lines was continually validated through immunofluorescence of SOX2 and Nanog (Fig. S1). Both hESCs and hiPSCs were cultured with defined Essential-8 (E8) media (made in house) on Matrigel® (Corning)-coated plates. Media was changed daily, and the cells were passaged every 3–4 days depending on confluency. For passaging, 0.5 mM EDTA (Corning) was used, and E8 media was supplemented with 5 μM Y27632 (Stem Cell Technologies) for 24 hr to enhance cell survival. Cells were cryopreserved in 90% FBS and 10% DMSO.

2.5. Human cardiac fibroblast culture

Human ventricular cardiac fibroblasts (hCFs) were purchased from Lonza and were grown in DMEM supplemented with 10% FBS (Thermo), 1% Penicillin/streptomycin (Thermo), and 1 ng/mL bFGF (PeproTech). hCFs were passaged with 0.05% Trypsin-EDTA (Thermo), and used for experiments from passage 4–10. hCFs were characterized for protein expression of vimentin (Vim) and connexin 43 (CX43), and validated for lack of differentiation to myofibroblasts, through α-smooth muscle actin (αSMA) expression (Fig. S2).

2.6. Human cardiomyocyte (hCM) differentiation

The differentiation protocol used for ventricular-specific hCMs from hPSCs involved the use of small molecule induction [8] and hCM selection through glucose starvation [12,52]. Specifically, after culture of hPSCs in E8 media until near confluency (~80%), the differentiation protocol was initiated by media change to RPMI + B27 minus insulin (RPMI, 2% B27 minus insulin, 1% Pen/strep), and activation of the Wnt pathway, through inhibition of the Glycogen Synthase Kinase-3 (GSK) pathway, with 12 μM CHIR99021 (BioVision) on day 0 (D0). After 24 hr of Wnt activation (D1), the media was changed to simply RPMI + B27 minus insulin to allow for cell recovery. At D3, half of the media was removed, and the rest of the media was resupplied as conditioned media, and the Wnt pathway was inhibited with 5 μM IWP-2 (Sigma). At D5, the media was changed to RPMI + B27 minus insulin for cell recovery. Then, D7 and D9, the media was changed to RPMI + B27 plus insulin (RPMI, 2% B27 plus insulin, 1% Pen/strep) to support cardiac maturation. At D11 and D14, the media was changed to RPMI without glucose + B27 plus insulin, supplemented with 4 mM sodium lactate and 1% pen/strep, to purify the population for hCMs [12]. Then, on D17 for cell recovery, the media was switched back to RPMI + B27 plus insulin. At D19, the purified hCMs were replated, with TrypLE Express (LifeTech) to lift cells onto new Matrigel®-coated plates, to remove dead cells and cell debris. At this point, hCMs were characterized (i.e. via flow cytometry and IF; Fig. S3) and were then used for the formation of 3D cardiac tissue within the microfluidic chip.

2.7. Formation and culture of 3D hPSC-CM tissue within the microfluidic chip

After differentiation and purification, the hCMs were prepared for use in 3D tissue experiments. Specifically, the wells were washed with 1X DPBS (Dulbecco's phosphate buffered solution), and the cells were lifted off with TrypLE Express (LifeTech) incubation following 37 °C for 10 min. Then, the cells were mechanically dissociated through pipetting up and down against the culture vessel, and the enzyme was buffered with RPMI + B27 plus insulin. The hCMs were centrifuged at 300 g for 3 min. The supernatant was aspirated, then the cell pellet was resuspended in RPMI + B27 plus insulin. Similarly, in parallel, hCFs were trypsinized and collected for device loading. Then, hCMs were mixed with hCFs at a 4:1 ratio (as determined through a series of optimization, and thus used for all subsequent experiments), mixed with collagen (final concentration 2 mg/mL), and 20% Matrigel®, rendering the final cell density as $35x10^6$ cells/mL. Cell-embedded hydrogel solution was mixed and subsequently injected into tissue region of microfluidic platforms (3 μL per device). Devices were flipped and incubated at 37 °C for 18 min for hydrogel polymerization, then RPMI + B27 plus insulin was injected into the flanking media channels. Media was changed everyday. Similarly, 4:1 CM:CF cell populations were plated in Matrigel®-coated 24-well plates for the age-matched monolayer experimental setting.

2.8. Microscopy

Phase contrast and fluorescence images were acquired using Zeiss Axio Observer Z1 equipped with Apotome2 (Zeiss) and ZenPro software. Throughout the cell culture period, samples were imaged every other day using phase contrast at a 10X objective. Time-lapse imaging was recorded at 10X objective for 30 s at 37 ˚C on day 14 to analyze spontaneous contraction of the 3D tissue inside the chip, including beats per minute (BPM) and inter-beat interval variability. To calculate inter-beat interval variability, the contraction peaks were extracted, and the time between beats was calculated using custom written Matlab codes, adapted from Refs. [53]. The standard deviation of the inter-beat interval was calculated and deemed the measure of inter-beat interval variability.

2.9. Immunofluorescence (IF)

For IF staining, samples were fixed in 4% paraformaldehyde (PFA) at day 14 of culture. The devices were incubated at 37 ˚C for 15 min. Afterwards, the cells were rinsed with PBS-glycine 2X for 10 min of incubation each at room temperature. The final wash was with PBS-Tween-20 ((PBS-Polyoxyethylene (20) sorbitan monolaurate) (0.05% (v/v) Polyoxyethylene (20) sorbitan monolaurate in PBS) for 10 min at room temperature. Then, the cells were permeablized with 0.1% Triton-X-100 for 30 min at room temperature. To inhibit non-specific binding of the antibodies, blocking was then performed with 10% goat serum solution for 1 hr at room temperature. To stain for cardiac-specific markers, the primary antibodies were diluted in 10% goat serum and added to the samples at 4 ˚C overnight. The following primary antibodies were used for IF staining: rabbit anti-SOX2 (Cell Signaling, 1:100), mouse anti-Nanog (Abcam, 1:200), rabbit anti-Connexin 43 (Abcam, 1:200), mouse anti-Sarcomeric α-actinin (Sigma, 1:200), rabbit anti-α smooth muscle actin (Abcam, 1:100), mouse anti-cTnT (Thermo, 1:200), mouse anti-von Willebrand Factor (Santa Cruz, 1:200), and rabbit anti-Vimentin (Cell Signaling, 1:250).

Upon addition of the primary antibodies, the following day, the samples were washed with PBS-Tween-20 three times for 20 mintues each at room temperature. Then, the secondary antibodies were diluted in PBS-Tween-20 (1:500), centrifuged at 14K RPM for 10 min, then added to the samples. After 30 min-1 hr, the samples were washed with PBS-Tween-20 three times for 10 min each at room temperature. To stain for the actin cytoskeleton and the nucleus, Alexa Fluor 488-or Alexa Fluor647-Phalloidin (1:40) and 4',6-diamidino-1-phenylindole (DAPI) (1:1000) were added to the samples and left at 4 ˚C overnight. Then the samples were washed with PBS-Tween-20 three times for 20 min each at room temperature. Finally, the samples were imaged using fluorescence microscopy (Zeiss Axio Observer Z1 with the Zen Pro software suite) equipped with Apotome2 at 10X, 20X, and 40X objectives and Z-stacked images were captured and reconstructed to form representative 3D images. Alternatively, samples were imaged with the Leica SP8 Confocal Microscope at 40X and 63X objectives, with z-stacked images captured and reconstructed to form representative 3D images.

2.10. Analysis of 3D cardiac tissue alignment

Tissues stained for F-actin and DAPI were used for assessment and calculation of cellular alignment. F-actin images were measured with FIJI software for Fast Fourier Transform (FFT), and DAPI images were used to quantify nuclei alignment [54]. Specifically, for calculation of alignment, images were rotated based on phase contrast to set alignment axis at 0°. DAPI images were thresholded, processed through the Watershed plugin, and the nuclei were analyzed through the Analyze Particles Plugin. Proportion of nuclei at each angle was calculated and graphed in a histogram with bins spanning 10°.

2.11. Quantitative real-time reverse transcription-PCR (qPCR)

Gene expression was performed on hESC-derived cardiac tissues for up to n = 4 experiments. Specifically, tissues within microfluidic chips were digested with 1 mg/mL collagenase type I (Alfa Aesar), and cells were collected from devices. Total RNA was extracted from cell suspension with Total RNA Microprep kit (Zymo). RNA quality and concentration were assessed with either High Sensitivity RNA tapes or Regular Sensitivity RNA tapes. cDNA was synthesized from total RNA using iScript Reverse Transcriptase Supermix (BioRad). iTaq Universal SYBR Green Supermix (BioRad) was used to perform qPCR on synthesized cDNA, with 18S as the housekeeping gene. Primers were validated via melt curve analysis and PCR product size verification. For qPCR, 8 μM dilution of forward and reverse primers was used for 10 μL reactions within 384-well plates, with 0.1 μL per of cDNA. The qPCR plates were analyzed with CFX384 Touch Real-Time PCR Detection System (BioRad).

2.12. Epinephrine testing

After spontaneous contractions were recorded as the baseline for day 14 of hiPSC-derived cardiac tissue culture within devices with and without posts, tissue responsiveness to epinephrine was evaluated. Specifically, epinephrine was first resuspended in 0.5 M HCl at 0.1 mg/mL, then it was diluted in RPMI + B27 plus insulin at a final concentration of 0.2 μg/mL and administered to the devices for 5 min at 37 ˚C [55]. Then, tissues were transferred to the Zeiss microscope for 30 s video recordings at 37 ˚C. Using the custom-written Matlab code, spontaneous BPM values were extracted for both baseline contraction and in response to epinephrine. The change in BPM in response to epinephrine dosing for each tissue was calculated.

2.13. Calcium transients

To assess calcium (Ca^{2+}) transients within engineered cardiac tissues, calcium indicator dye, Fluo-4AM assay kit (LifeTech), was used. Specifically, on day 14 of culture, tissues in devices both with and without posts were incubated with calcium indicator solution (50 μg of Fluo-4AM in 50 μL of Pluronic F127), in a dilution of 10 μL in 1 mL of DPBS 1X, for 40 min at 37 ˚C. Then, devices were washed with media (RPMI + B27 plus insulin) for 25 min at 37 ˚C, then 10 μM of blebbistatin was diluted in Tyrode's solution and incubated for 5 min to reduce motion artifacts. Then, tissues were transferred to the microscope, maintained at 37 ˚C, and imaged with Zeiss fluorescent microscope (at 25.23 frames/sec) at 488 nm wavelength. Movies were recorded for a duration of 30 s, and calcium concentration changes were calculated by normalizing the fluorescent dye intensity (F) during cells' contractions to the background intensity (F_0) and plotted over time [50].

2.14. Statistical analysis

Paired, two-sided t-tests were used for statistical analysis of calculated final CM:CF ratios, inter-beat interval variability, and BPM for each condition using R. For gene expression data, two-way ANOVA was performed on the DCT values from qPCR data, using GraphPad Prism. Two-way ANOVA was performed using GraphPad Prism on the tissue alignment and thickness analysis.

3. Results and discussion

3.1. Development of the microfluidic chip for generation of 3D aligned cardiac tissue

The 3D anisotropic architecture of the myocardium is highly correlated to its function; a key component that is missing in most of the

microfluidic platforms. Throughout development, the human myocardium experiences a complex myriad of stimuli that induce transcriptional, electrophysiological, and structural changes, resulting in aligned tissue architecture [24,31,56]. Although the exact sequence of events and related mechanisms that occur during development to induce tissue-level anisotropy are unknown, electrical and mechanical stimulation have been demonstrated *in vitro* to affect cardiac alignment. Similarly, micropatterning in the form of ECM printing and surface topography also enhances tissue-level alignment. Particularly, microposts have been demonstrated to serve as mesoscopic topographical cues that induce cell elongation and alignment similar to that seen in the native developing myocardium when implemented in 3D cell culture [41]. Despite this, none of the existing microfluidic platforms for hPSC-CM culture have incorporated microposts as topography within the main tissue region to induce 3D cellular anisotropy. To that end, we incorporated and optimized staggered microposts within the central tissue chamber of the fabricated microfluidic platform to provide a highly controllable environment that favors induction of 3D cardiac tissue anisotropy. Through formation of repeated elliptical pores that force cells via passive tension to shape around the pore boundaries [57], the model serves to replicate the highly anisotropic nature of the human myocardium (Fig. 1A and B). The 3D tissue region was surrounded by media channels to allow for nutrient and oxygen diffusion. Specifically, the tissue region was separated from the flanking outer channels through borders of trapezoidal posts, that contain the hydrogel while allowing media diffusion [58], regularly spaced at 100 μm with heights and lengths of 100 μm and 200 μm, respectively. Simulation of diffusion of 10 kDa FITC-conjugated Dextran was performed with COMSOL Multiphysics® to ensure proper diffusion of molecules applied from the flanking media channels throughout tissue (Fig. 1C). Simulation results demonstrated that the array of trapezoidal posts around the hydrogel allowed diffusion across the interface of the media channels and the 3D hydrogel-encapsulated tissue, creating a concentration gradient that levels out 3 hr after supplementation. In order to evaluate possible functionalities of the enclosed microfluidic device with perfusable media on diffusion of nutrients through the encapsulated cardiac tissue, we further performed simulation 10 kDa FITC-conjugated Dextran (Fig. S4) under constant fluid flow through the media channels. Compared to stagnant media supplementation, it appeared that continuous media exchange resulted in enhanced diffusion to the tissue region by the 3 hr time point. Thus, further targeted studies utilizing this platform could take advantage of the intrinsic properties of its microfluidic nature to establish dynamic culture conditions, and study effects of enhanced nutrient supplementation on cardiac tissue function. However, the scope of this manuscript herein is the creation, optimization, and extensive characterization of the proposed novel microfluidic chip with innate microposts to culture engineered cardiac tissue, therefore media was set to be stagnant and changed every 24 hr. Additionally, stagnant media supplementation necessitates a much simpler set up as it does not require extensive pumping or tubing, thus rendering the use of device easier and more adaptable for several biological studies.

3.2. Generation of 3D aligned neonatal rat cardiac tissue within the microfluidic chip

We hypothesized that the 3D co-culture of hydrogel-encapsulated cardiac cells, within a microfluidic platform with precise architecture to induce tissue anisotropy over extended culture, would serve to mature the cardiac tissue. In order to test this, we performed our initial experiments using neonatal rat cardiac cells. To form the tissue, we specifically utilized a combined culture of rCMs and rCFs, as the co-culture of these cells better mimics the composition of the myocardium, through coordination of electrical and mechanical signal propagation and ECM deposition [13]. The co-culture of rCMs and rCFs was incorporated within various microfluidic chip designs to determine optimal parameters for the formation of 3D mature cardiac tissue, including hydrogel composition, cellular co-culture ratio, culture time, and precise device architecture (i.e. channel size and width, micropost geometry and distance). Specifically, hydrogel compositions that were tested include mixtures of fibrin, collagen, and Matrigel®. Co-culture ratios tested were 1:0, 8:1, and 4:1 CM:CF. In order to isolate the optimal architecture of the microfluidic platform, in addition to different micropost shapes (elliptical vs. hexagonal), the sizes of the microposts (200–800 μm long, 100–300 μm wide), and the staggering of the microposts (vertical post spacing: 100–300 μm, horizontal post spacing: 100–300 μm) were further studied. Within the microfluidic platforms with innate microposts, the 3D encapsulated cardiac tissues compacted the hydrogel and formed elliptical pores around the designated microposts, that varied in size and shape along with varying device design parameters. Formation of these pores induced high cell alignment around the pore boundaries, while enhancing cell elongation and nutrient diffusion across the tissue region (refer to Fig. 1B).

Based on a series of initial experiments to enhance cell elongation and tissue formation, the optimal hydrogel composition and co-culture ratio for rCMs were found to be 85:15 of fibrin (2 mg/mL): collagen (1 mg/mL), and 4:1 CM:CF, respectively (data not shown). Dimensions of the microposts identified as optimal for tissue anisotropy were 500 μm long and 100 μm wide, with horizontal post spacing (hPS) as 150 μm. With determined hydrogel, co-culture ratio, and micropost dimensions remaining constant, iterations of device designs were tested, by varying the micropost geometry (i.e. elliptical vs. hexagonal) as well as vertical post spacing (vPS) (Fig. 2A). Co-culture of cardiac cells encapsulated within a fibrin:collagen hydrogel was injected into designs with hexagonal or elliptical microposts, with varying vPS of 150 or 200 μm, and tissue architecture and function after two weeks of

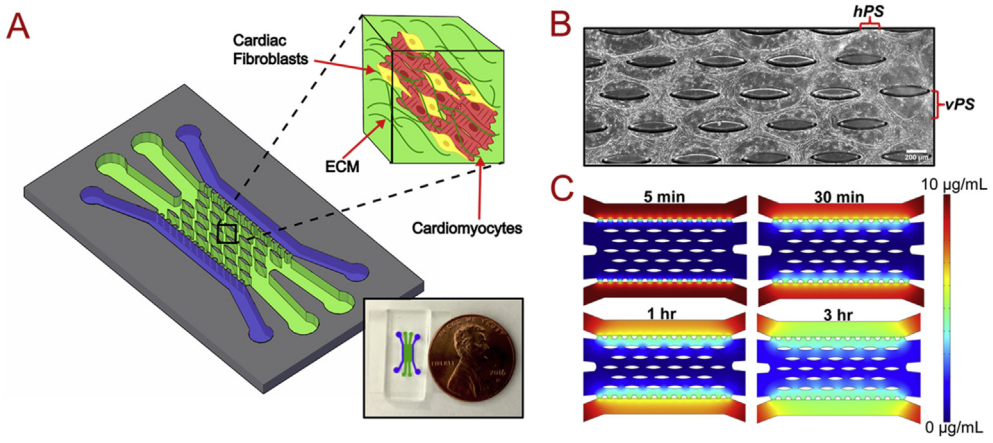

Fig. 1. Microfluidic chip for 3D cardiac tissue modeling: (A) Schematic of the microfluidic chip with inset of US penny for scaling. (B) Phase contrast image of cardiac tissues formed in device, with horizontal post spacing (hPS) and vertical post spacing (vPS) defined. (C) Simulation of 10 kDa Dextran diffusion from media to tissue channels, demonstrating the concentration gradient over time.

A

Design #	Micropost shape	Vertical post spacing (μm)
1	Elliptical	200
2	Elliptical	150
3	Hexagonal	200
4	Hexagonal	150

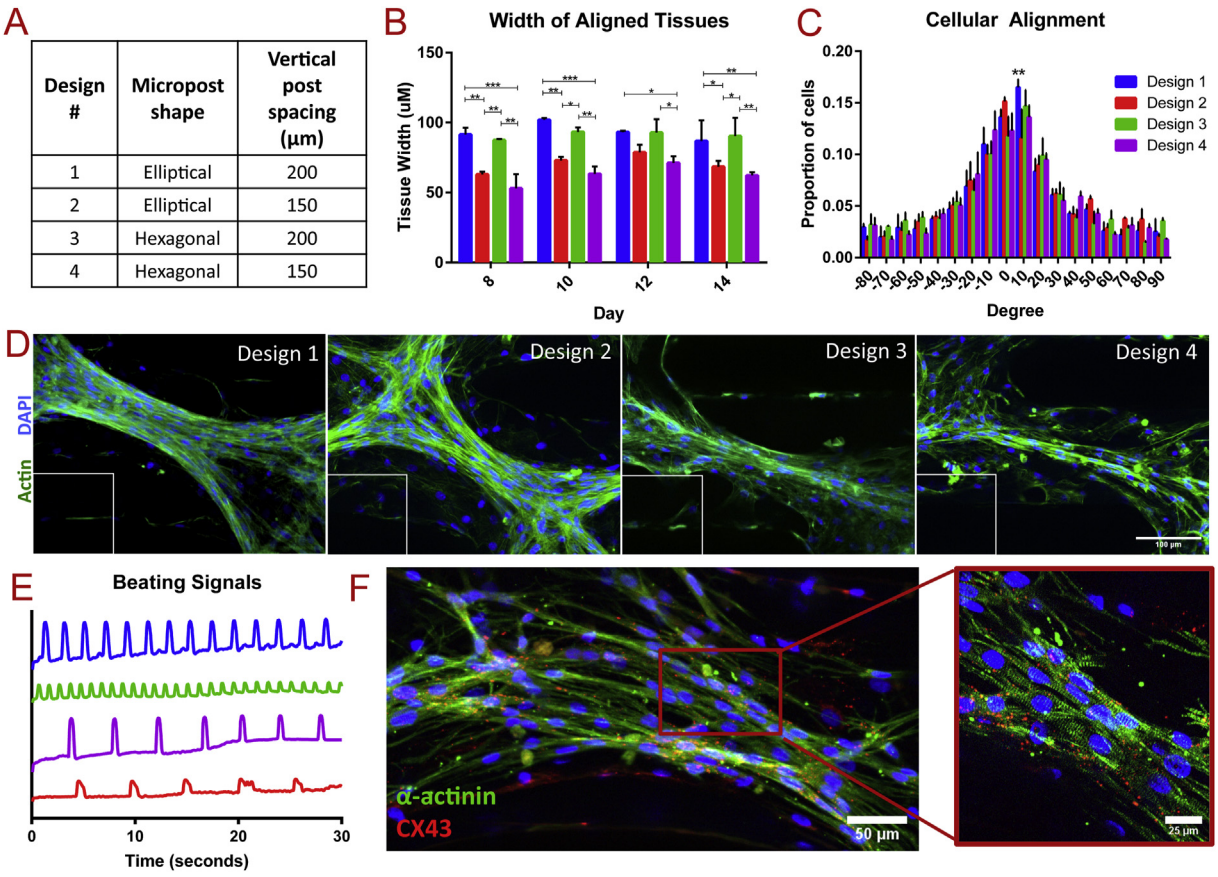

Fig. 2. Optimization of microfluidic chip design parameters with neonatal rat cardiac cells: (A) Table of microfluidic chip designs with differing post dimensions. (B–F) Characterization of neonatal rat cardiac tissue within each design. (B) Tissue width, (C) cellular alignment, (D) immunostaining of actin and DAPI with inset as FFT, and (E) representative beating signals from tissues formed within each device. (F) Cardiac-specific marker staining of tissues in Design 1, demonstrating aligned sarcomeres (green) and abundant, localized connexin 43 (red), with 40X magnification to right. Statistics performed on two-way ANOVA of (B) n = 2 experiments and (C) n = 3 experiments. (For interpretation of the references to colour in this figure legend, the reader is referred to the Web version of this article.)

culture were assessed. Specifically, width of tissues, alignment of cells, and spontaneous contractions were analyzed throughout the culture period (14 days). The width of aligned tissues between microposts for each design remained consistent from day 8 to day 14 of culture, however the vPS had a significant effect on width of resultant tissues (Fig. 2B). The designs with 200 μm vPS exhibited tissue bundles with the largest widths (Designs 1 and 3), while the designs with 150 μm vPS exhibited smaller width tissues (Designs 2 and 4). Nuclear alignment analysis of immunostained tissues at day 14 highlighted a significant increase in proportion of cells aligned along the alignment axis from 0 to 10° in Design 1, than all other designs (Fig. 2C), as corroborated through cytoskeletal F-actin fiber staining of cardiac tissues and corresponding FFT analysis (Fig. 2D, Fig. S5A). Particularly, the devices with elliptical microposts (Designs 1 and 2) formed tissues with enhanced integrity, demonstrated through denser tissue bundles in IF of F-actin, than the devices with the hexagonal posts (Designs 3 and 4). In addition, anisotropic tissues formed within Design 1 (device with elliptical posts and 200 μm vPS) also demonstrated more synchronous contractile patterns on day 14, as identified through signal extraction via a custom written Matlab code from spontaneous beating videos (Fig. 2E, Movies S1-4). Correspondingly, highly aligned sarcomeric striations and abundant CX43 expression (Fig. 2F, Fig. S5B) were identified to a greater degree in this design than in tissues formed within other designs. Therefore, the particular dimensions of the innate micropost array within Design 1 induced formation of anisotropic co-cultured cardiac tissues, with corresponding enhanced cardiac-marker expression and spontaneous contractile behavior. To that end, Design 1 was chosen as the optimal microfluidic chip design for the formation of human-derived 3D cardiac tissues and all subsequent experimental studies.

Supplementary video related to this article can be found at https://doi.org/10.1016/j.biomaterials.2020.120195

3.3. Cardiomyocyte differentiation and purification from hESCs and hiPSCs

For the formation of 3D cardiac tissues within the optimized design, we differentiated hCMs from monolayers of both hESCs and hiPSCs. The differentiation was performed through activation of the canonical Wnt signaling pathway by inhibition of GSKβ followed by sequential inhibition of Wnt [8]. Typically, spontaneous beating initiated from D7-11 of culture. Metabolic selection, based on glucose starvation, was performed from D11-D17 to enrich for hCMs [12]. After metabolic selection, the hCMs were replated to eliminate dead cells and debris. Flow cytometry analysis revealed high percentages of hCMs, with a representative flow cytometry histogram in Fig. 3A showing a cardiac differentiation at 90.8% $cTnT^+$, and an average overall differentiation efficiency of 85.5% $cTnT^+$ cells. This data was further corroborated with high GFP expression in hCMs differentiated from transduced hESCs with GFP linked under the cTnT promoter, and IF staining for cTnT among hiPSC-CMs (Fig. S3). hCMs differentiated from hESCs and hiPSCs reveal indistinguishable morphologies and protein expression as demonstrated in Fig. 3B–D. The resultant tissue populations reveal islands of dense hCM populations (sarcomeric α-actinin $(SAA)^+$), with surrounding populations of isolated non-myocytes (Vim^+). IF

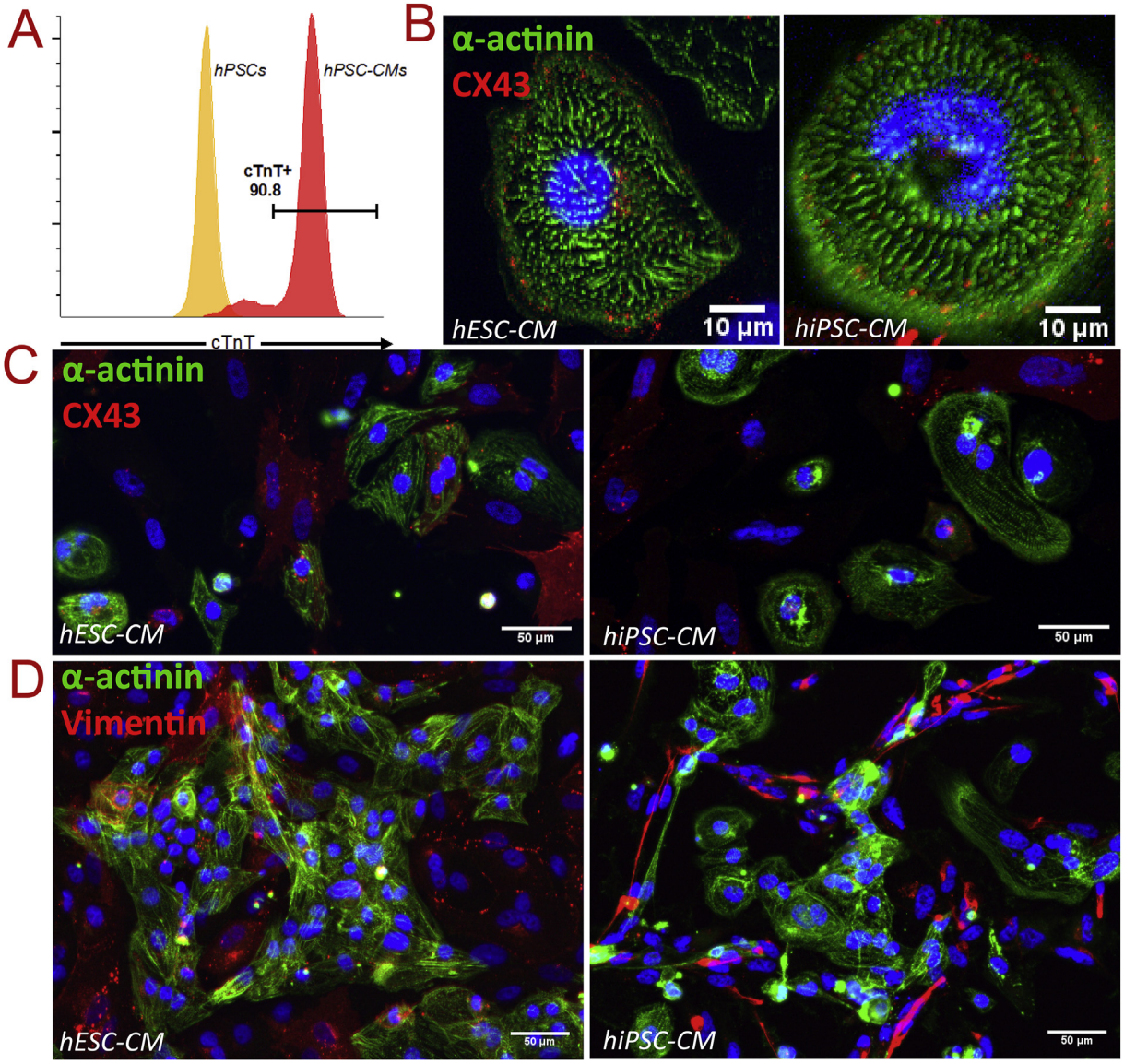

Fig. 3. Characterization of human cardiomyocytes (hCMs) differentiated from both hESCs and hiPSCs: (A) Flow cytometry plot of differentiated hCM population, showing > 90% cTnT expression. (B) Cardiac-specific expression staining for SAA (green) and CX43 (red) of hESC (left) and hiPSC (right) differentiated hCMs at 40X, and at 20X in (C). (D) Immunostaining of SAA (green) and Vim (red) for identification of hCMs and non-CMs, respectively. (For interpretation of the references to colour in this figure legend, the reader is referred to the Web version of this article.)

characterization of the non-CMs, consistent with previous work [14], revealed 65.86% CFs (vWF^-/Vim^+) and 31.24% ECs (vWF^+/Vim^+). The combined strategy for differentiation and purification led to consistent, highly pure hCM populations, that were subsequently incorporated into the optimized microfluidic chip.

3.4. Generation of 3D organized cardiac tissues from human stem cells

To test formation of 3D human cardiac tissue within the microfluidic chip, the differentiated and purified hCMs were mixed with hCFs (as characterized in Fig. S2), embedded into fibrin:collagen hydrogel, and injected into the optimized microfluidic device of Design 1. The optimal conditions for 3D tissue formation, as identified with rat cardiac cell culture, were initially tested for the creation of human cardiac tissue from hPSC-CMs. Specifically, the culture duration and device design values were kept consistent. The co-culture ratio was again validated with hPSC-CMs, demonstrating enhanced alignment with tissues formed with 4:1 CM:CF over 8:1 and 1:0 CM:CF (Fig. S6). To that end, our data strongly suggests that the co-culture ratio of 4:1 CM:CF optimized with rat tissues was equally optimal for human cardiac tissue formation, and was thus sustained for all subsequent experiments. However, due to low gel compaction and significant variation in gelling times, the hydrogel formulation was changed to a mixture of collagen type I (2 mg/mL) and Matrigel® at a ratio of 80:20 as it showed highest cell elongation, consistency and easier handling, and better represented the adult myocardium, as its main ECM component is collagen [59]. In addition, cell density was slightly increased (from 30 to $35x10^6$ cells/mL). Apart from devices embedded with microposts, devices of identical design, except lacking the microposts, were fabricated in order to serve as 3D co-culture controls, to specifically isolate the effect of micropost presence on tissue formation, alignment, and function.

After two weeks of culture, IF staining of cardiac tissues within both types of devices (i.e. with and without the posts) was performed, to assess cardiac tissue composition, integrity, and structure, as well as individual cell structure (Fig. 4). The tissues formed within devices without the posts exhibited random, unorganized structure in both hESC- and hiPSC-derived cardiac tissues, as demonstrated through F-actin cytoskeletal staining and corresponding FFT analysis (Fig. 4A).

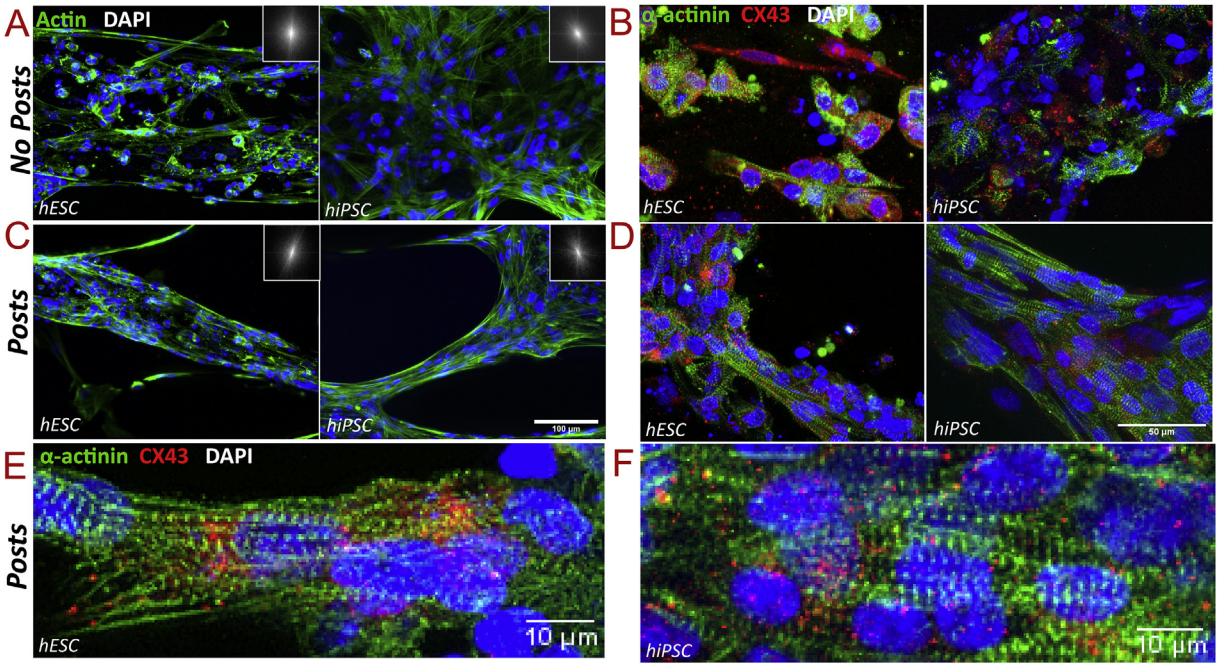

Fig. 4. Structural properties of human stem cell-derived cardiac tissues formed within microfluidic devices with and without the microposts: (A, B) Tissues in devices without the microposts, showing cytoskeleton through immunostaining of (A) actin and DAPI and (B) cardiac-specific markers through immunostaining of SAA and CX43. (C–F) Tissues in devices with the posts, showing (C) cytoskeleton and (D-F) cardiac-specific markers. Magnified view of sarcomere alignment and CX43 expression of (E) hESC- and (F) hiPSC-derived tissue within devices with posts.

Additionally, cardiac-specific marker staining revealed round hCMs with disarrayed sarcomeres and non-localized CX43 in these no-post devices (Fig. 4B), a phenotype consistent with immature hCMs [24]. However, the tissues formed within devices with the posts notably exhibited highly aligned structure, as demonstrated from F-actin staining and FFT analysis (Fig. 4C). Additionally, two weeks of culture within the device was sufficient in attaining a similar degree of anisotropy as when culture was extended to three weeks, since level of tissue alignment within each respective condition (i.e. with or without posts) was sustained. This confirmed that the day 14 experimental time point was appropriate to achieve the high level of anisotropy within the device with posts to perform functional and molecular-level analyses. In addition, tissues formed within devices with posts at both time points were significantly more aligned than either time point of no post conditions (Fig. S7).

Further analysis of anisotropic tissues formed within devices with the microposts revealed that the cells exhibited organized cytoskeletons, elongated structure, abundant striated sarcomeres, and localized CX43 expression along the cell border (Fig. 4D–F), regardless of location among posts. Notably, tissues within the vertical spacing of posts were highly aligned and condensed (Fig. S8A), in contrast with the formation of nodes of cardiac tissue in the horizontal spacing between posts (Fig. S8B). To determine the composition of the cardiac populations at day 14, IF was performed to distinguish the hCFs/non-CMs from the hCMs, through positive staining for Vim and SAA, respectively. hCFs were identified throughout the tissue within both types of devices, moreso than in 2D space-limited monolayer conditions. Specifically, cell population composition of cardiac tissues was quantified based on IF in each condition and lower CM:CF ratios were demonstrated in devices with and without posts (Figs. S9A–D, p-value for posts to 2D as 0.1201, p-value for posts to no posts as 0.1338, p-value for no posts to 2D as 0.3328). Additionally, IF revealed that hCFs had proliferated onto the surrounding glass and PDMS, both within the tissue region and in the inlet/outlet ports of both types of devices (Figs. S9B–C). These values were omitted in CM:CF ratio quantification, as only the areas of the device with the hydrogel-encapsulated cardiac tissue were imaged and considered.

The reason for resultant decreased CM:CF ratio within the 3D device conditions, and maintenance of CM:CF ratio in age-matched 2D culture after the two-week period, can be hypothesized to be due to multiple factors. First, the cell population is cultured at maximum confluency in 2D, thereby it is expected that the fibroblasts undergo contact inhibition and arrest their proliferation [60], leading to maintenance of initial cell composition. Secondly, fibroblasts are sensitive to mechanical stress and may respond to stretch within the 3D ECM in device conditions, which in turn activates various pathways, leading to proliferation, deposition of ECM, and release of growth factors [61]. Thirdly, CMs have also been demonstrated to release growth factors in response to stretch, that in turn induce fibroblast responses, normally attributed to CF response to mechanical stimulation, such as proliferation, ECM deposition, and gene expression regulation [61,62]. Therefore, the CFs may be experiencing multiple stimuli within the 3D culture environment of the microfluidic platform which upregulate their proliferation, while the CFs in 2D experience contact inhibition and halt proliferative processes, leading to the observed decrease in CM:CF ratio in 3D, and, on the other hand, maintained cellular ratio in 2D upon two weeks of culture.

3.5. Gene expression analysis of human cardiac tissues

Upon formation and assessment of the phenotype of 3D human tissue within the microfluidic chip, gene expression analysis was performed to assess changes in tissue-level transcription, as an indicator for maturation state, due to extended culture within each condition. To serve as a population control, gene expression values were compared to the respective cardiac cell population immediately before insertion into the device (deemed as D0). In addition, monolayers of 4:1 CM:CF were cultured in standard Matrigel®-coated 2D plates for the experimental period (i.e. 14 days) to serve as age-matched 2D comparison to the tissues formed within devices (Fig. 5A). The panel of genes that were assayed includes those important for cardiac tissue function and structure. The genes were broadly classified as involved in either

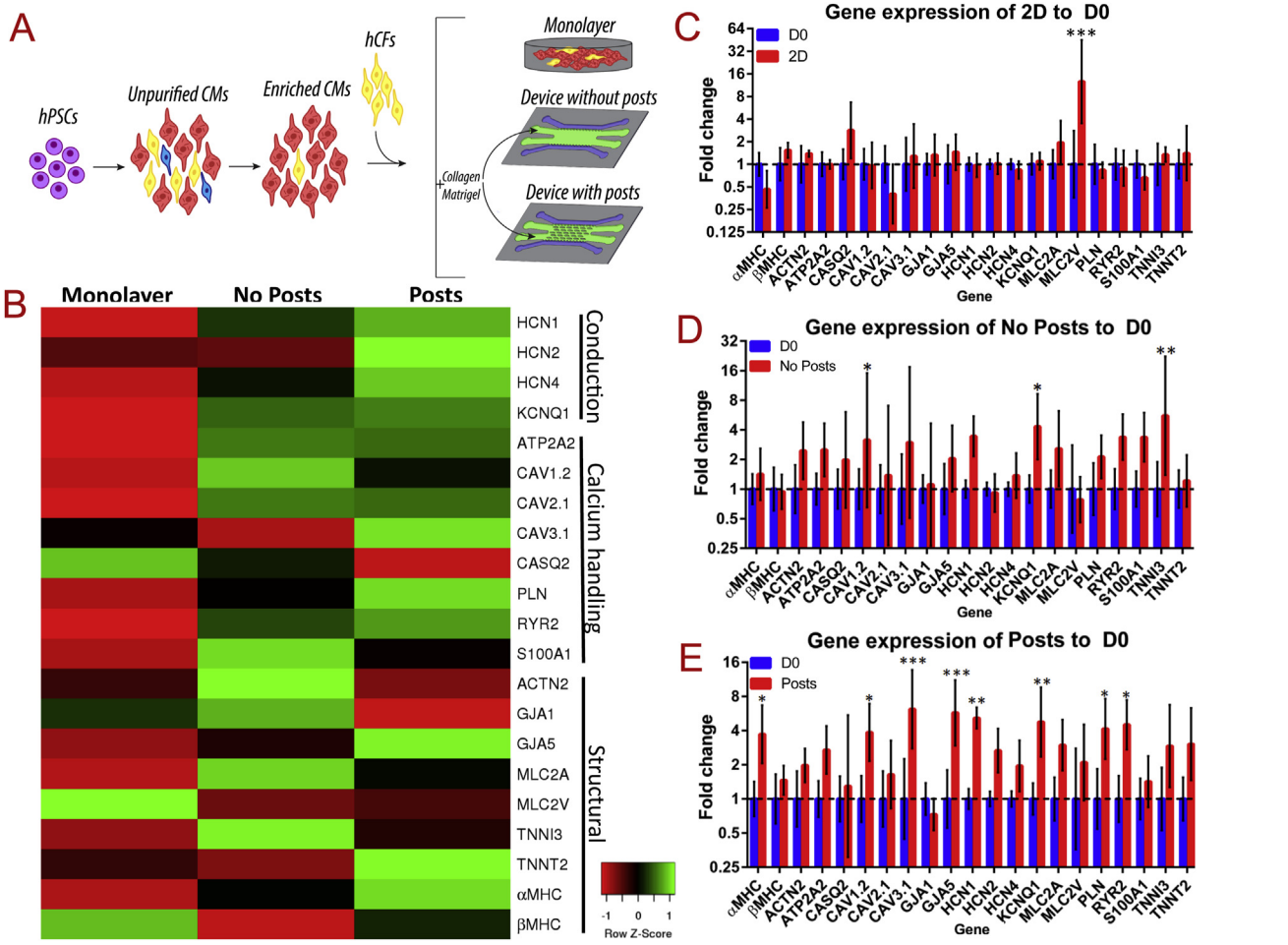

Fig. 5. Gene expression analysis of human stem cell-derived cardiac tissues in monolayer and microfluidic chips: (A) Schematic of formation of tissues within devices and age-matched monolayer. (B) Heatmap of fold changes of all conditions to D0, with z-score displayed. (C) Gene expression of 2D age-matched monolayers compared to before insertion. (D) Gene expression of tissues in devices without posts compared to before insertion (D0). (E) Gene expression of tissues in devices with posts compared to before insertion (D0). Statistics performed on ANOVA of DCT values of $n \leq 4$ experiments, with p-values: * < 0.05, ** < 0.01, *** < 0.001.

calcium handling, structural, or conduction, in order to isolate the biological processes that may be affected. Incorporated in this panel were maturation-specific genes, deemed as those demonstrated with significantly higher expression in adult over fetal hearts and hPSC-CMs, including: ACTN2, ATP2A2, CASQ2, CAV1.2, CAV3.1, HCN1, HCN4, KCNQ1, MYH7, PLN, RYR2, S100A1, TNNI3, and TNNT2 [24,27]. Average values of fold change from D0 of tissues from devices with posts, without posts, and age-matched 2D monolayers were plotted in an expression heatmap, with row z-score displayed (Fig. 5B). Overall, the 3D tissues formed within the microfluidic chip, both with and without posts, demonstrate more upregulation of genes than those in the 2D monolayer, suggesting that 3D hydrogel and co-culture with hCFs over two weeks influences genes important in cardiac function. Specifically, tissues in age-matched 2D monolayers only displayed a significant upregulation of MLC2V (Fig. 5C). This result coincides with the findings that co-culture of hCMs with hCFs, as well as extended culture time, promote a more mature hCM phenotype [63].

Within devices without posts in comparison to D0, tissues demonstrated an upregulation in some cardiac-related genes, with significant upregulation in the conduction maker KCNQ1, calcium handling marker CAV1.2, and structural marker TNNI3 (Fig. 5D). In order to investigate the additional effect of anisotropy on cardiac tissues within identical 3D hydrogel culture and CF presence, gene expression of tissues formed within the microfluidic chip with posts, in comparison to D0, was further analyzed. These highly aligned cardiac tissues within our microfluidic chip exhibited extensive significant upregulation, particularly in "maturation-specific" genes (Fig. 5E). These genes included HCN1, KCNQ1, CAV1.2, CAV3.1, PLN, and RYR2 [27], which participate in calcium handling and conduction-specific processes. Therefore, the engineered cardiac tissues within our 3D microfluidic chip demonstrated an upregulation in both calcium handling and conduction processes, with significant trends demonstrated particularly for maturation-specific genes. These results correspond to the exhibited enhanced cell and tissue structure due to induction of 3D tissue anisotropy, revealing the capability to mature hPSC-derived cardiac tissue within our microfluidic chip. Additionally, expression levels of some structural-specific genes were significantly upregulated, including GJA5 and αMHC. GJA5 translates CX40, which has been demonstrated between CF:CF and CM:CF junctions [64]. Therefore, upregulation of GJA5 may signify higher presence of hCFs in 3D device conditions, which is corroborated with presence of more fibroblasts/non-myocytes through IF staining of Vim and the resultant decrease in calculated CM:CF ratio in 3D conditions (Figs. S9B–D). In contrast, αMHC expression decreases during heart development, which is inconsistent with our model, as well as many other *in vitro* models, highlighting the future need to investigate myosin isoform switching, and how it can be better replicated *in vitro* [26,28]. On the other hand, we demonstrate an average elevated expression in devices with posts of βMHC (not significant), which predominates in the adult heart.

In order to specifically identify effect of microposts on tissue function, tissues grown in devices with and without the posts were directly compared. Although more genes were significantly upregulated in the

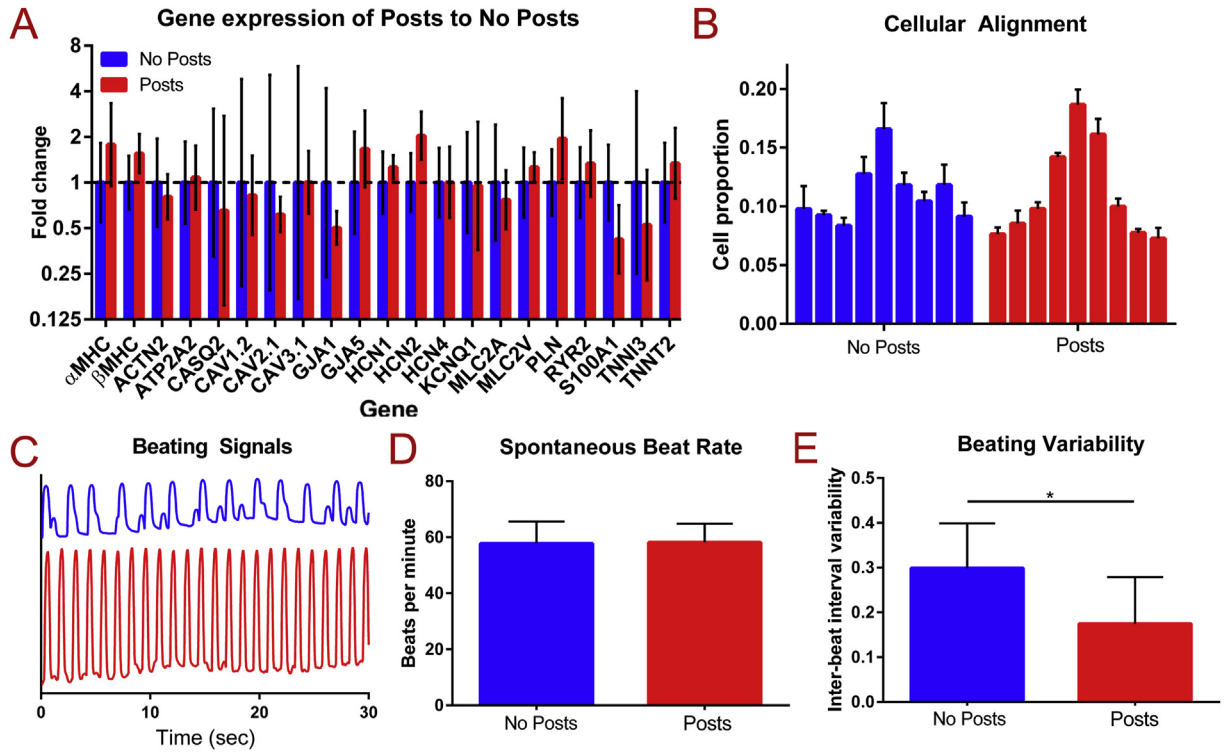

Fig. 6. Comparison of human cardiac tissues cultured in devices with and without microposts: (A) Gene expression, (B) cellular alignment, (C) representative spontaneous beating signals, (D) spontaneous beating rate, and (E) beating variability, calculated by inter-beat interval variability, of tissues grown for two weeks in devices with and without posts. Statistics performed on ANOVA of hESC and hiPSC tissues for (B) n = 5 experiments and for (D) and (E) n = 10 experiments, with * denoting p-value < 0.05.

post condition than in no posts condition in comparison to D0, gene expression between devices with and without posts was not significantly different for the chosen panel when the device conditions are directly compared (Fig. 6A). However, tissues in the devices with posts demonstrated a more normal distribution of cell alignment around the alignment axis (at 0°) than the no post condition, suggesting a higher degree of anisotropy in tissues formed within devices with posts (Fig. 6B), due to the formation of repeated pores throughout the tissue that also enhance media and thus nutrient/oxygen diffusion. The enhanced cell and tissue structure and corresponding protein expression reveal that although the microposts do not appear to affect expression of the genes that were analyzed, they play a pertinent role in cardiac tissue structure and formation that may affect tissue function. To that end, we further investigated spontaneous beating signals as a characteristic of tissue function from real-time videos of tissues in post and no post conditions (Fig. 6C, Movies S5-7). The peaks of tissue contraction from these signals were extracted to determine spontaneous beat rate and inter-beat interval variability, deemed a measure of spontaneous contraction synchronicity. Tissues grown within both types of chips (i.e. with and without the posts) exhibited similar physiologically relevant beating rates, regardless of chip design (Fig. 6D). However, significantly larger inter-beat interval variability, or more inconsistent contraction patterns, was demonstrated in tissues grown in devices without posts in comparison to those with posts (p-value of 0.0300) (Fig. 6E). This finding demonstrates that the contractile function of these tissues differs based solely on chip design.

Supplementary video related to this article can be found at https://doi.org/10.1016/j.biomaterials.2020.120195

To further investigate the tissue functionality, spontaneous calcium transients were recorded and analyzed for hPSC-derived 3D cardiac tissues formed after two weeks of culture within the microfluidic devices with and without posts. Within each recorded tissue area, the fluorescent intensity of calcium spikes (F) for five regions of interest was divided by background intensity (F_0) and plotted over a period of 30 s (Fig. 7A and B). The resultant calcium transients revealed highly variable calcium release patterns for tissues within devices without posts, that were asynchronous among the different subregions (Fig. 7A, Supplementary Movie 8). On the other hand, tissues developed within devices with posts demonstrated extremely consistent calcium transients, that were synchronous to the calcium spikes of all other subregions (Fig. 7B, Supplementary Movie 9). These findings further confirm that the microfluidic chip promotes enhanced cell-cell communication and electrical signal propagation. Specifically, in direct comparison to an isotropic 3D control, engineered anisotropic tissues demonstrated calcium handling properties and spontaneous contractions with enhanced synchronicity, revealing the particular effects of topography-induced alignment on tissue maturation.

Supplementary video related to this article can be found at https://doi.org/10.1016/j.biomaterials.2020.120195

Furthermore, the responsiveness of the engineered cardiac tissues was tested through administration of the β-adrenergic agonist, epinephrine (i.e. adrenaline), to probe the physiological relevancy of the 3D formed tissue within the platform and its capabilities for drug response studies. Both tissues formed within devices with and without the posts demonstrated a positive chronotropic effect to epinephrine dosing (Fig. 7C), however tissues within the posts condition exhibited more organized spontaneous contraction patterns in response to epinephrine in comparison to tissues within devices without posts. Additionally, the tissues developed within the demonstrated microfluidic device with posts responded to epinephrine dosing with a significantly higher change in BPM than tissues in the no posts condition (p-value of 0.04056) (Fig. 7D), demonstrating enhanced clinical relevancy of the proposed microfluidic model.

Therefore, tissues formed in devices with posts exhibited enhanced synchronicity, presenting more connected and thus augmented electrophysiological function, which may be due to the enhanced

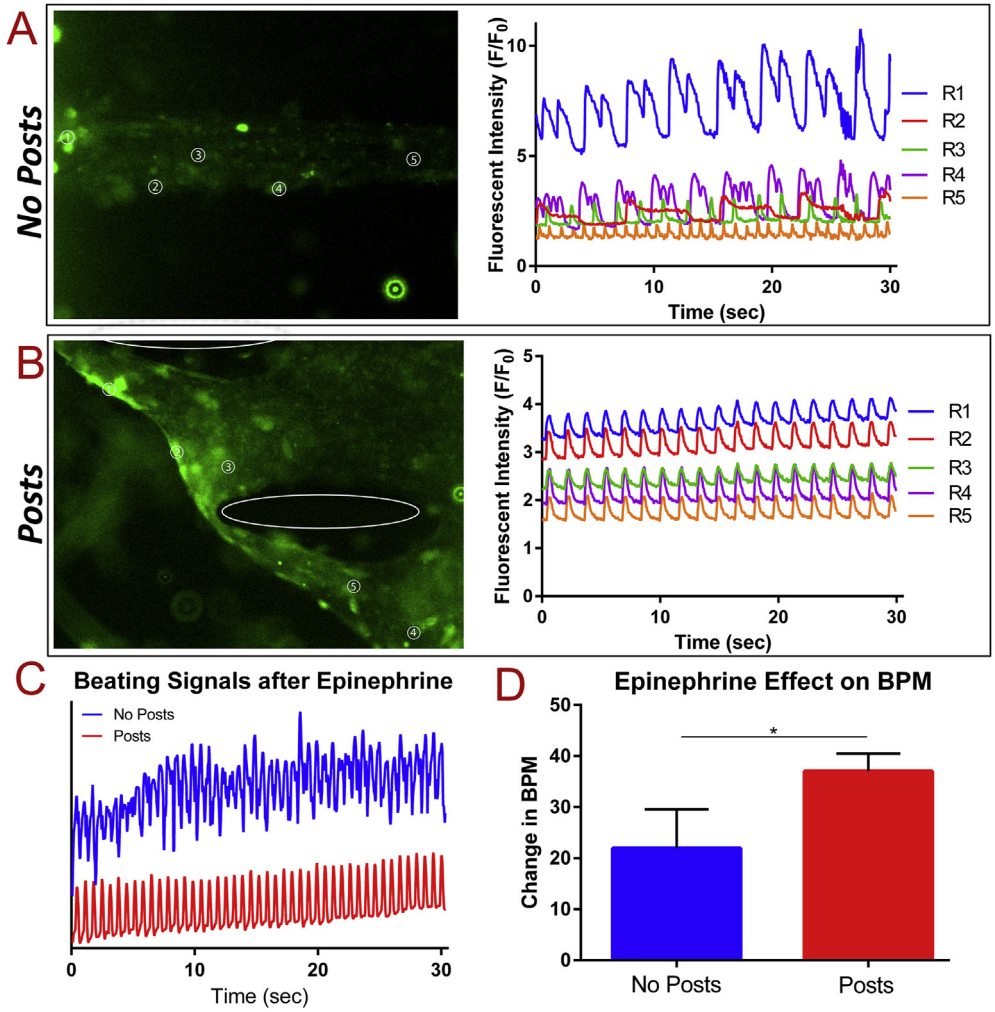

Fig. 7. Functional assessment of human stem cell-derived cardiac tissues within devices with and without posts after 14 days of culture: Calcium transients and extracted related frequency signals of intracellular change in concentration of Ca^{2+} for (A) devices without posts and (B) devices with posts, with R1-R5 representing regions 1–5. (C-D) Responsiveness of tissues to epinephrine, with (C) representative beating signals(, and (D) corresponding changes in spontaneous BPM. Statistics were performed through two-sided, paired *t*-test of n = 3 experiments of hiPSC-derived tissues, with * denoting p-value < 0.05.

localization of gap junctions and coordinated tissue structure. This suggests that the cells in devices with posts undergo mechanotransduction, initiated from the interaction with the microposts, inducing changes either a) of translational and/or post-translational levels of particular proteins, or b) of the transcription of alternative genes that were not studied herein and require further analysis. The cells that comprised tissues formed among the microposts demonstrated elongated shape, therefore it is also plausible that pathways involved in physiologic hypertrophy are activated [65,66]. Likewise, as focal adhesions connect the ECM to the cytoskeleton and are involved in promoting and directing myofibril assembly [17,65], the presence of extensive sarcomere alignment in microfluidic chips with the microposts suggests that processes involving focal adhesion kinases (FAKs) are specifically influenced within this culture condition. Particularly, in response to the stretch sensed from micropost-induced pore formation, stretch-related receptors such as integrins may be activated, that in turn signal certain kinases, among such are FAKs and mitogen-activated protein kinases (MAPKs) [66–68]. Signaling by these different kinases generally leads to a cascade of events, including activation of various proteins that activate transcription factors that translocate to the nucleus to ultimately affect gene transcription. Therefore, it is plausible that transcription of specific genes affected through these mechanotransduction-related pathways, in addition to available levels of related proteins, are influenced in the different chip conditions. The exact mechanism that connects micropost-guided alignment and enhanced contractile function will be a suitable subject of future study. Nevertheless, due to the combination of anisotropic structure, 3D culture, and exposure to supporting cells (CFs), tissues formed in devices with the microposts exhibit the most significant upregulation of an abundance of cardiac-specific maturation genes in comparison to D0 tissues, demonstrating with elongated CMs, striated parallel sarcomeres, localized gap junction staining, and synchronous whole-tissue contraction. Additionally, tissues within these devices demonstrate physiologically relevant functionalities, as revealed through synchronous calcium transients, and positive chronotropy in response to β-adrenergic agonist.

Future works could further improve the proposed *in vitro* platform for enhanced functional measurements particularly for those of great importance to cardiac tissue studies, such as contractile force measurements. In order to fulfill the needs for real-time measurement of force in disease modeling and pharmaceutical testing applications, an innate method to measure contractile force is of great importance. Future works shall investigate the use of innate, free-standing micropillar arrays, capable of force measurement, similar to the approach described in Ref. [21], within the microfluidic device to allow for real-time force monitoring. Additionally, methods will be investigated to enhance the platform's ability to model the adult myocardium, such as induction of a pronounced myosin isoform switch from β to α. For

example, sustained electrical conditioning has been demonstrated to enhance the electrophysiology and transcriptional signature of hPSC-derived CMs. However, a rather complicated setup is necessary to incorporate sustained external stimulation, and our model is advantageous in its low cost and ease of creation. Similarly, an enlarged version of the platform could be constructed to allow for a large cell population to select for CMs for downstream analyses, however such a platform would negate the many advantages of a microfluidic platform, i.e. high throughput, minimal cell/reagent necessary, and reduced variation with input differentiation populations. To further take advantage of the microfluidic nature of the described platform, a future work could also involve implantation of continuous fluid flow through the media channels to enable enhanced nutrient supply and dynamic culture conditions, which have recently been demonstrated to enhance cardiac tissue function [69]. Thus, with the many advantages of the proposed platform, taken together with the demonstrated ability to mature and enhance cardiac tissue formation, the design presented herein has great potential for physiologically relevant disease modeling. As this platform has been validated for use with CMs differentiated from hiPSCs, there exists the possibility in future works to model genetic diseases through CRISPR/Cas9 gene editing, as well as patient-specific diseases, through reprogramming of patient fibroblasts to hiPSCs. Additionally, the microfluidic nature of the platform allows for the implementation of precise molecular gradients, as observed throughout native tissues and organs, therefore allowing diseases derived from external insult (i.e. hypoxia, drugs, stimulants) to be modeled. The enhanced mature nature of the tissue provides a model with more physiological relevance than 2D-cultured hPSC-derived CMs to the human myocardium.

4. Conclusions

In this study, we demonstrated the precise design of a microfluidic platform for successful 3D cardiac tissue formation and function, developed first with rat-derived cardiac cells, and then validated with both hESC- and hiPSC-derived CMs. To enhance the physiological complexity, CMs were co-cultured with interstitial CFs within hydrogels embedded in the platform, resulting in cardiac tissues with a high degree of cellular interconnectivity and functionality, as demonstrated through gap junction localization, sarcomere organization and synchronicity in spontaneous contraction. Importantly, incorporation of complex 3D micropost architecture within the tissue region of the microfluidic chip significantly enhanced the tissue organization, with the added potential for high throughput experimentation with minimal necessary cells and corresponding reagents. We demonstrated extensive characterization of co-cultured anisotropic cardiac tissues grown for up to three weeks within the proposed microfluidic chip design. Our results highlighted that the formed tissues within the chip exhibited mature cellular structure, protein expression as well as an upregulation of genes with roles in tissue structure, calcium handling, and electrical conduction. Interestingly, incorporation of the mesoscopic microposts led to significantly enhanced tissue function as evidenced by increased synchronicity of spontaneous beating, calcium transients, and enhanced response to β-adrenergic agonist. In summary, 3D cardiac tissues formed within the proposed microfluidic chip presented with enhanced structure, function and physiological relevancy that surpass conventional 2D monolayer culture assays, therefore highlighting the great potential of this platform for future disease modeling and predictive drug testing studies.

CRediT authorship contribution statement

Jaimeson Veldhuizen: Conceptualization, Methodology, Validation, Formal analysis, Investigation, Data curation, Writing - original draft, Writing - review & editing, Visualization. **Joshua Cutts:** Methodology, Validation, Investigation, Formal analysis, Writing - review & editing. **David A. Brafman:** Conceptualization, Resources, Writing - review & editing. **Raymond Q. Migrino:** Conceptualization, Methodology, Supervision, Writing - review & editing. **Mehdi Nikkhah:** Conceptualization, Methodology, Resources, Writing - review & editing, Supervision, Project administration, Funding acquisition.

Declaration of competing interest

The authors declare that they have no known competing financial interests or personal relationships that could have appeared to influence the work reported in this paper.

Acknowledgements

We would like to thank NSF CAREER Award #1653193, Arizona Biomedical Research Commission (ABRC) New Investigator Award (ADHS18-198872), and the Flinn Foundation for providing funding sources for this project. We would like to thank Prof. Michael Caplan who provided us with an analytical workstation for COMSOL Multiphysics® modeling. We would also like to thank Zachery Camacho and Maria Soldevila for their help in microfluidic device fabrication, Eric Barrientos for his help in schematic preparation, and Ali Navaei for his help in neonatal rat cell isolation.

Appendix A. Supplementary data

Supplementary data to this article can be found online at https://doi.org/10.1016/j.biomaterials.2020.120195.

References

[1] P.A. Heidenreich, J.G. Trogdon, O.A. Khavjou, J. Butler, K. Dracup, M.D. Ezekowitz, E.A. Finkelstein, Y. Hong, S.C. Johnston, A. Khera, D.M. Lloyd-Jones, S.A. Nelson, G. Nichol, D. Orenstein, P.W. Wilson, Y.J. Woo, C. American Heart Association Advocacy Coordinating, C. Stroke, R. Council on Cardiovascular, Intervention, C. Council on Clinical, E. Council on Prevention, A. Council on, B. Vascular Thrombosis, C. Council on, C. Critical, Perioperative, N. Resuscitation, D. Council on Cardiovascular, S. Council on the Kidney in Cardiovascular, Council on Cardiovascular, C. Anesthesia, Interdisciplinary Council on Quality of R Outcomes, Forecasting the future of cardiovascular disease in the United States: a policy statement from the American Heart Association, Circulation 123 (8) (2011) 933–944.

[2] D. Rajamohan, E. Matsa, S. Kalra, J. Crutchley, A. Patel, V. George, C. Denning, Current status of drug screening and disease modelling in human pluripotent stem cells, Bioessays 35 (3) (2013) 281–298.

[3] P. Liang, K. Sallam, H. Wu, Y. Li, I. Itzhaki, P. Garg, Y. Zhang, V. Vermglinchan, F. Lan, M. Gu, T. Gong, Y. Zhuge, C. He, A.D. Ebert, V. Sanchez-Freire, J. Churko, S. Hu, A. Sharma, C.K. Lam, M.M. Scheinman, D.M. Bers, J.C. Wu, Patient-specific and genome-edited induced pluripotent stem cell-derived cardiomyocytes elucidate single-cell phenotype of brugada syndrome, J. Am. Coll. Cardiol. 68 (19) (2016) 2086–2096.

[4] N. Sun, M. Yazawa, J. Liu, L. Han, V. Sanchez-Freire, O.J. Abilez, E.G. Navarrete, S. Hu, L. Wang, A. Lee, A. Pavlovic, S. Lin, R. Chen, R.J. Hajjar, M.P. Snyder, R.E. Dolmetsch, M.J. Butte, E.A. Ashley, M.T. Longaker, R.C. Robbins, J.C. Wu, Patient-specific induced pluripotent stem cells as a model for familial dilated cardiomyopathy, Sci. Transl. Med. 4 (130) (2012) 130–147.

[5] L. Guo, R.M. Abrams, J.E. Babiarz, J.D. Cohen, S. Kameoka, M.J. Sanders, E. Chiao, K.L. Kolaja, Estimating the risk of drug-induced proarrhythmia using human induced pluripotent stem cell-derived cardiomyocytes, Toxicol. Sci. 123 (1) (2011) 281–289.

[6] G. Wang, M.L. McCain, L. Yang, A. He, F.S. Pasqualini, A. Agarwal, H. Yuan, D. Jiang, D. Zhang, L. Zangi, J. Geva, A.E. Roberts, Q. Ma, J. Ding, J. Chen, D.Z. Wang, K. Li, J. Wang, R.J. Wanders, W. Kulik, F.M. Vaz, M.A. Laflamme, C.E. Murry, K.R. Chien, R.I. Kelley, G.M. Church, K.K. Parker, W.T. Pu, Modeling the mitochondrial cardiomyopathy of Barth syndrome with induced pluripotent stem cell and heart-on-chip technologies, Nat. Med. 20 (6) (2014) 616–623.

[7] D. Mosqueira, I. Mannhardt, J.R. Bhagwan, K. Lis-Slimak, P. Katili, E. Scott, M. Hassan, M. Prondzynski, S.C. Harmer, A. Tinker, J.G.W. Smith, L. Carrier, P.M. Williams, D. Gaffney, T. Eschenhagen, A. Hansen, C. Denning, CRISPR/Cas9 editing in human pluripotent stem cell-cardiomyocytes highlights arrhythmias, hypocontractility, and energy depletion as potential therapeutic targets for hypertrophic cardiomyopathy, Eur. Heart J. 39 (43) (2018) 3879–3892.

[8] X. Lian, J. Zhang, S.M. Azarin, K. Zhu, L.B. Hazeltine, X. Bao, C. Hsiao, T.J. Kamp, S.P. Palecek, Directed cardiomyocyte differentiation from human pluripotent stem cells by modulating Wnt/beta-catenin signaling under fully defined conditions, Nat. Protoc. 8 (1) (2013) 162–175.

[9] K. Ban, S. Bae, Y.S. Yoon, Current strategies and challenges for purification of cardiomyocytes derived from human pluripotent stem cells, Theranostics 7 (7) (2017) 2067–2077.

[10] H. Uosaki, H. Fukushima, A. Takeuchi, S. Matsuoka, N. Nakatsuji, S. Yamanaka, J.K. Yamashita, Efficient and scalable purification of cardiomyocytes from human embryonic and induced pluripotent stem cells by VCAM1 surface expression, PloS One 6 (8) (2011) e23657.

[11] N.C. Dubois, A.M. Craft, P. Sharma, D.A. Elliott, E.G. Stanley, A.G. Elefanty, A. Gramolini, G. Keller, SIRPA is a specific cell-surface marker for isolating cardiomyocytes derived from human pluripotent stem cells, Nat. Biotechnol. 29 (11) (2011) 1011-U82.

[12] A. Sharma, G. Li, K. Rajarajan, R. Hamaguchi, P.W. Burridge, S.M. Wu, Derivation of highly purified cardiomyocytes from human induced pluripotent stem cells using small molecule-modulated differentiation and subsequent glucose starvation, Jove-J Vis Exp 97 (2015).

[13] M. Radisic, H. Park, S. Gerecht, C. Cannizzaro, R. Langer, G. Vunjak-Novakovic, Biomimetic approach to cardiac tissue engineering, Philos. Trans. R. Soc. Lond. B Biol. Sci. 362 (1484) (2007) 1357–1368.

[14] D. Zhang, I.Y. Shadrin, J. Lam, H.Q. Xian, H.R. Snodgrass, N. Bursac, Tissue-engineered cardiac patch for advanced functional maturation of human ESC-derived cardiomyocytes, Biomaterials 34 (23) (2013) 5813–5820.

[15] K. Ronaldson-Bouchard, S.P. Ma, K. Yeager, T. Chen, L. Song, D. Sirabella, K. Morikawa, D. Teles, M. Yazawa, G. Vunjak-Novakovic, Advanced maturation of human cardiac tissue grown from pluripotent stem cells, Nature 556 (7700) (2018) 239–243.

[16] M. Valderrabano, Influence of anisotropic conduction properties in the propagation of the cardiac action potential, Prog. Biophys. Mol. Biol. 94 (1–2) (2007) 144–168.

[17] M.A. Bray, S.P. Sheehy, K.K. Parker, Sarcomere alignment is regulated by myocyte shape, Cell Motil. Cytoskelet. 65 (8) (2008) 641–651.

[18] A. Agarwal, J.A. Goss, A. Cho, M.L. McCain, K.K. Parker, Microfluidic heart on a chip for higher throughput pharmacological studies, Lab Chip 13 (18) (2013) 3599–3608.

[19] I.Y. Shadrin, B.W. Allen, Y. Qian, C.P. Jackman, A.L. Carlson, M.E. Juhas, N. Bursac, Cardiopatch platform enables maturation and scale-up of human pluripotent stem cell-derived engineered heart tissues, Nat. Commun. 8 (1) (2017) 1825.

[20] S.S. Nunes, J.W. Miklas, J. Liu, R. Aschar-Sobbi, Y. Xiao, B. Zhang, J. Jiang, S. Masse, M. Gagliardi, A. Hsieh, N. Thavandiran, M.A. Laflamme, K. Nanthakumar, G.J. Gross, P.H. Backx, G. Keller, M. Radisic, Biowire: a platform for maturation of human pluripotent stem cell-derived cardiomyocytes, Nat. Methods 10 (8) (2013) 781–787.

[21] S. Schaaf, A. Shibamiya, M. Mewe, A. Eder, A. Stohr, M.N. Hirt, T. Rau, W.H. Zimmermann, L. Conradi, T. Eschenhagen, A. Hansen, Human engineered heart tissue as a versatile tool in basic research and preclinical toxicology, PloS One 6 (10) (2011) e26397.

[22] O. Binah, K. Dolnikov, O. Sadan, M. Shilkrut, N. Zeevi-Levin, M. Amit, A. Danon, J. Itskovitz-Eldor, Functional and developmental properties of human embryonic stem cells-derived cardiomyocytes, J. Electrocardiol. 40 (6 Suppl) (2007) S192–S196.

[23] M. Snir, I. Kehat, A. Gepstein, R. Coleman, J. Itskovitz-Eldor, E.G. Livne, Assessment of the ultrastructural and proliferative properties of human embryonic stem cell-derived cardiomyocytes, Am. J. Physiol. Heart Circ. Physiol. 285 (2003) 2355–2363.

[24] X. Yang, L. Pabon, C.E. Murry, Engineering adolescence: maturation of human pluripotent stem cell–derived cardiomyocytes, Circ. Res. (2014) 511–523.

[25] C.C. Veerman, G. Kosmidis, C.L. Mummery, S. Casini, A.O. Verkerk, M. Bellin, Immaturity of human stem-cell-derived cardiomyocytes in culture: fatal flaw or soluble problem? Stem Cell. Dev. 24 (9) (2015) 1035–1052.

[26] C.Y. Ivashchenko, G.C. Pipes, I.M. Lozinskaya, Z. Lin, X. Xiaoping, S. Needle, E.T. Grygielko, E. Hu, J.R. Toomey, J.J. Lepore, R.N. Willette, Human-induced pluripotent stem cell-derived cardiomyocytes exhibit temporal changes in phenotype, Am. J. Physiol. Heart Circ. Physiol. 305 (6) (2013) H913–H922.

[27] Y. Jiang, P. Park, S.M. Hong, K. Ban, Maturation of cardiomyocytes derived from human pluripotent stem cells: current strategies and limitations, Mol. Cell 41 (7) (2018) 613–621.

[28] S.D. Lundy, W.Z. Zhu, M. Regnier, M.A. Laflamme, Structural and functional maturation of cardiomyocytes derived from human pluripotent stem cells, Stem Cell. Dev. 22 (14) (2013) 1991–2002.

[29] Y. Zhao, N. Rafatian, N.T. Feric, B.J. Cox, R. Aschar-Sobbi, E.Y. Wang, P. Aggarwal, B. Zhang, G. Conant, K. Ronaldson-Bouchard, A. Pahnke, S. Protze, J.H. Lee, L. Davenport Huyer, D. Jekic, A. Wickeler, H.E. Naguib, G.M. Keller, G. Vunjak-Novakovic, U. Broeckel, P.H. Backx, M. Radisic, A platform for generation of chamber-specific cardiac tissues and disease modeling, Cell 176 (4) (2019) 913-927 e18.

[30] N.N. Chattergoon, G.D. Giraud, S. Louey, P. Stork, A.L. Fowden, K.L. Thornburg, Thyroid hormone drives fetal cardiomyocyte maturation, Faseb. J. 26 (1) (2012) 397–408.

[31] C. Kim, M. Majdi, P. Xia, K.A. Wei, M. Talantova, S. Spiering, B. Nelson, M. Mercola, H.S. Chen, Non-cardiomyocytes influence the electrophysiological maturation of human embryonic stem cell-derived cardiomyocytes during differentiation, Stem Cell. Dev. 19 (6) (2010) 783–795.

[32] T.J. Herron, A.M. Rocha, K.F. Campbell, D. Ponce-Balbuena, B.C. Willis, G. Guerrero-Serna, Q. Liu, M. Klos, H. Musa, M. Zarzoso, A. Bizy, J. Furness, J. Anumonwo, S. Mironov, J. Jalife, Extracellular matrix-mediated maturation of human pluripotent stem cell-derived cardiac monolayer structure and electrophysiological function, Circ Arrhythm Electrophysiol 9 (4) (2016) e003638.

[33] H. Saini, A. Navaei, A. Van Putten, M. Nikkhah, 3D cardiac microtissues encapsulated with the co-culture of cardiomyocytes and cardiac fibroblasts, Adv Healthc Mater 4 (13) (2015) 1961–1971.

[34] J. Veldhuizen, R.Q. Migrino, M. Nikkhah, Three-dimensional microengineered models of human cardiac diseases, J. Biol. Eng. 13 (2019) 29.

[35] B.W. Ellis, A. Acun, U.I. Can, P. Zorlutuna, Human iPSC-derived myocardium-on-chip with capillary-like flow for personalized medicine, Biomicrofluidics 11 (2) (2017) 024105.

[36] A. Mathur, P. Loskill, K. Shao, N. Huebsch, S. Hong, S.G. Marcus, N. Marks, M. Mandegar, B.R. Conklin, L.P. Lee, K.E. Healy, Human iPSC-based cardiac microphysiological system for drug screening applications, Sci. Rep. 5 (2015) 8883.

[37] O. Mastikhina, B. Moon, K. Williams, R. Hatkar, D. Gustafson, O. Mourad, X. Sun, M. Koo, A. Lam, Y. Sun, J. Fish, E. Young, S.S. Nunes, Human cardiac fibrosis-on-a-chip model recapitulates disease hallmarks and can serve as a platform for drug testing, Biomaterials 233 (2019).

[38] F. Laco, T.L. Woo, Q. Zhong, R. Szmyd, S. Ting, F.J. Khan, C.L.L. Chai, S. Reuveny, A. Chen, S. Oh, Unraveling the inconsistencies of cardiac differentiation efficiency induced by the GSK3beta inhibitor CHIR99021 in human pluripotent stem cells, Stem Cell Reports 10 (6) (2018) 1851–1866.

[39] G. Bergstrom, J. Christoffersson, K. Schwanke, R. Zweigerdt, C.F. Mandenius, Stem cell derived in vivo-like human cardiac bodies in a microfluidic device for toxicity testing by beating frequency imaging, Lab Chip 15 (15) (2015) 3242–3249.

[40] C. Zuppinger, 3D cardiac cell culture: a critical review of current technologies and applications, Front Cardiovasc Med 6 (2019) 87.

[41] W. Bian, B. Liau, N. Badie, N. Bursac, Mesoscopic hydrogel molding to control the 3D geometry of bioartificial muscle tissues, Nat. Protoc. 4 (10) (2009) 1522–1534.

[42] D. Truong, J. Puleo, A. Llave, G. Mouneimne, R.D. Kamm, M. Nikkhah, Breast cancer cell invasion into a three dimensional tumor-stroma microenvironment, Sci. Rep. 6 (2016) 34094.

[43] S. Nagaraju, D. Truong, G. Mouneimne, M. Nikkhah, Microfluidic tumor–vascular model to study breast cancer cell invasion and intravasation, Adv Healthc Mater 7 (9) (2018).

[44] N. Peela, E.S. Barrientos, D. Truong, G. Mouneimne, M. Nikkhah, Effect of suberoylanilide hydroxamic acid (SAHA) on breast cancer cells within a tumor–stroma microfluidic model, Int. Biodeterior. 9 (12) (2017).

[45] D.D. Truong, A. Kratz, J.G. Park, E.S. Barrientos, H. Saini, T. Nguyen, B. Pockaj, G. Mouneimne, J. LaBaer, M. Nikkhah, A human organotypic microfluidic tumor model permits investigation of the interplay between patient-derived fibroblasts and breast cancer cells, Canc. Res. 79 (12) (2019) 3139–3151.

[46] C.R. Kothapalli, P. Honarmandi, Theoretical and experimental quantification of the role of diffusive chemogradients on neuritogenesis within three-dimensional collagen scaffolds, Acta Biomater. 10 (8) (2014) 3664–3674.

[47] C. Wang, H. Lu, M.A. Schwartz, A novel in vitro flow system for changing flow direction on endothelial cells, J. Biomech. 45 (7) (2012) 1212–1218.

[48] A. Navaei, N. Moore, R.T. Sullivan, D. Truong, R.Q. Migrino, M. Nikkhah, Electrically conductive hydrogel-based micro-topographies for the development of organized cardiac tissues, RSC Adv. 7 (6) (2017) 3302–3312.

[49] A. Navaei, K. Rahmani Eliato, R. Ros, R.Q. Migrino, B.C. Willis, M. Nikkhah, The influence of electrically conductive and non-conductive nanocomposite scaffolds on the maturation and excitability of engineered cardiac tissues, Biomater Sci 7 (2) (2019) 585–595.

[50] A. Navaei, H. Saini, W. Christenson, R.T. Sullivan, R. Ros, M. Nikkhah, Gold nanorod-incorporated gelatin-based conductive hydrogels for engineering cardiac tissue constructs, Acta Biomater. 41 (2016) 133–146.

[51] A. Navaei, D. Truong, J. Heffernan, J. Cutts, D. Brafman, R.W. Sirianni, B. Vernon, M. Nikkhah, PNIPAAm-based biohybrid injectable hydrogel for cardiac tissue engineering, Acta Biomater. 32 (2016) 10–23.

[52] S. Tohyama, F. Hattori, M. Sano, T. Hishiki, Y. Nagahata, T. Matsuura, H. Hashimoto, T. Suzuki, H. Yamashita, Y. Satoh, T. Egashira, T. Seki, N. Muraoka, H. Yamakawa, Y. Ohgino, T. Tanaka, M. Yoichi, S. Yuasa, M. Murata, M. Suematsu, K. Fukuda, Distinct metabolic flow enables large-scale purification of mouse and human pluripotent stem cell-derived cardiomyocytes, Cell Stem Cell 12 (1) (2013) 127–137.

[53] S.B. Kim, H. Bae, J.M. Cha, S.J. Moon, M.R. Cokmeci, D.M. Croek, A. Khademhosseini, A cell-based biosensor for real-time detection of cardiotoxicity using lensfree imaging, Lab Chip 11 (10) (2011) 1801–1807.

[54] M.J. Raymond Jr., P. Ray, G. Kaur, A.V. Singh, L.Q. Wan, Cellular and nuclear alignment analysis for determining epithelial cell chirality, Ann. Biomed. Eng. 44 (5) (2016) 1475–1486.

[55] R.K. Birla, G.H. Borschel, R.G. Dennis, D.L. Brown, Myocardial engineering in vivo: formation and characterization of contractile, vascularized three-dimensional cardiac tissue, Tissue Eng. 11 (5–6) (2005) 803–813.

[56] R.S. Martherus, S.J. Vanherle, E.D. Timmer, V.A. Zeijlemaker, J.L. Broers, H.J. Smeets, J.P. Geraedts, T.A. Ayoubi, Electrical signals affect the cardiomyocyte transcriptome independently of contraction, Physiol. Genom. 42A (4) (2010) 283–289.

[57] W. Bian, C.P. Jackman, N. Bursac, Controlling the structural and functional anisotropy of engineered cardiac tissues, Biofabrication 6 (2) (2014) 024109-24109.

[58] C.P. Huang, J. Lu, H. Seon, A.P. Lee, L.A. Flanagan, H.Y. Kim, A.J. Putnam, N.L. Jeon, Engineering microscale cellular niches for three-dimensional multicellular co-cultures, Lab Chip 9 (12) (2009) 1740–1748.

[59] J.P. Guyette, J.M. Charest, R.W. Mills, B.J. Jank, P.T. Moser, S.E. Gilpin, J.R. Gershlak, T. Okamoto, G. Gonzalez, D.J. Milan, G.R. Gaudette, H.C. Ott, Bioengineering human myocardium on native extracellular matrix, Circ. Res. 118 (1) (2016) 56–72.

[60] H. Eagle, E.M. Levine, Growth regulatory effects of cellular interaction, Nature (1967) 1102–1106.

[61] P. Camelliti, T.K. Borg, P. Kohl, Structural and functional characterisation of cardiac fibroblasts, Cardiovasc. Res. 65 (1) (2005) 40–51.
[62] D. MacKenna, S.R. Summerour, F.J. Villarreal, Role of mechanical factors in modulating cardiac fibroblast function and extracellular matrix synthesis, Cardiovasc. Res. 46 (2) (2000) 257–263.
[63] I.C. Parrag, P.W. Zandstra, K.A. Woodhouse, Fiber alignment and coculture with fibroblasts improves the differentiated phenotype of murine embryonic stem cell-derived cardiomyocytes for cardiac tissue engineering, Biotechnol. Bioeng. 109 (3) (2012) 813–822.
[64] R.D. Johnson, P. Camelliti, Role of non-myocyte gap junctions and connexin hemichannels in cardiovascular health and disease: novel therapeutic targets? Int. J. Mol. Sci. 19 (3) (2018).
[65] D.E. Jaalouk, J. Lammerding, Mechanotransduction gone awry, Nat. Rev. Mol. Cell Biol. 10 (1) (2009) 63–73.
[66] W. Stansfield, M. Ranek, A. Pendse, J. Schisler, S. Wang, T. Pulinilkunnil, M. Willis, The Pathophysiology of Cardiac Hypertrophy and Heart Failure, Cellular and Molecular Pathobiology of Cardiovascular Disease, (2014), pp. 51–78.
[67] F.S. Pasqualini, A.P. Nesmith, R.E. Horton, S.P. Sheehy, K.K. Parker, Mechanotransduction and metabolism in cardiomyocyte microdomains, BioMed Res. Int. 2016 (2016) 4081638.
[68] M. Nikkhah, E. Edalat, S. Manoucheri, A. Khademhosseini, Engineering microscale topographies to control the cell–substrate interface, Biomaterials 33 (21) (2012).
[69] C.P. Jackman, A.L. Carlson, N. Bursac, Dynamic culture yields engineered myocardium with near-adult functional output, Biomaterials 111 (2016) 66–79.